ACS APPLIED MATERIALS & INTERFACES

Research Article

www.acsami.org

A Comparative Study of Layered Transition Metal Oxide Cathodes for Application in Sodium-Ion Battery

Ivana Hasa,[†] Daniel Buchholz,[‡,§] Stefano Passerini,*[,‡,§] and Jusef Hassoun*[,†]

[†]Department of Chemistry, Sapienza University of Rome, Piazzale Aldo Moro, 5, 00185 Rome, Italy

[‡]Helmholtz Institute Ulm, Helmholtzstraße 11, 89081 Ulm, Germany

[§]Karlsruher Institute of Technology (KIT), P.O. Box 3640, 76021 Karlsruhe, Germany

ABSTRACT: Herein, we report a study on P-type layered sodium transition metal-based oxides with a general formula of Na_xMO_2 (M = Ni, Fe, Mn). We synthesize the materials via coprecipitation followed by annealing in air and rinsing with water, and we examine the electrodes as cathodes for sodium-ion batteries using a propylene carbonate-based electrolyte. We fully investigate the effect of the Ni-to-Fe ratio, annealing temperature, and sodium content on the electrochemical performances of the electrodes. The impact of these parameters on the structural and electrochemical properties of the materials is revealed by X-ray diffraction, scanning electron microscopy, and cyclic voltammetry, respectively. The suitability of this class of P-type materials for sodium battery application is finally demonstrated by cycling tests revealing an excellent electrochemical performance in terms of delivered capacity (i.e., about 200 mAh g^{-1}) and charge−discharge efficiency (approaching 100%).

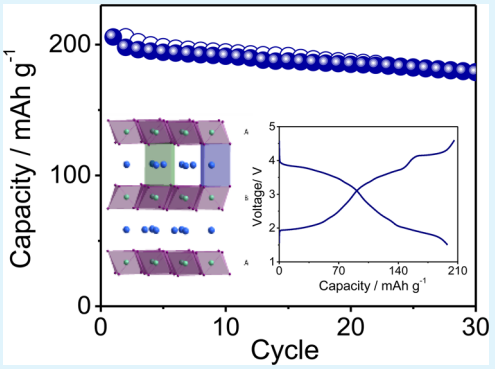

KEYWORDS: *Na_xMO_2 (M = Ni,Fe,Mn), cathode, P2−P3-type layered structure, sodium-ion, battery*

INTRODUCTION

Energy conversion and storage is one of the great challenges of the last decades. Hence, efficient, safe, low-cost, and environmentally friendly storage systems are required in response to modern society's needs. Li-ion batteries (LIBs) are considered one of the most promising systems to fulfill these requirements. In fact, they represent the most widespread secondary battery for consumer and portable electronics and are considered very promising candidates for power hybrid and electric vehicles.[1,2] Nevertheless, the market and the applications for rechargeable batteries are highly diversified and various requirements must be fulfilled. Stationary energy storage in contrast to high-energy applications is mainly driven by cost-efficient energy storage, which already points out that alternative battery chemistries complementary to and not competing with the lithium-ion battery technology are necessary.[3,4] Sodium-ion batteries have the potential to fulfill these criteria and match the economic and environmental issues due to the high abundance and low cost of the employed materials.[5,6]

Research on sodium-ion-based batteries has been conducted in parallel with lithium systems since the beginning of the 1980s;[7−10] however, the superior electrochemical performances led to a focus on LIBs. New Na-ion systems have attracted the interest of the broad scientific community again, with particular attention devoted to the study of intercalation and insertion materials. Indeed, suitable, high-performance cathodes and alternative anodes replacing the reactive metallic sodium have been discovered.[11−15]

Considering the large ionic radius of sodium and its preference for 6-fold coordination, like octahedral or prismatic sites, polyanionic networks and layered oxides appeared to be the most appropriate positive active materials. Research on the intercalation chemistry of sodium into layered oxides with the general formula Na_xMO_2 (M = transition metal) started around 1980,[16] when the classification of the structure according to the stacking arrangement of the metal oxide layers was also developed.[17] These layered materials consist of MO_6 edge-sharing octahedral units forming $(MO_2)_n$ sheets, between which the sodium cation is coordinated octahedral (O), tetrahedral (T), or prismatic (P). O-type layered oxides comprise sodium ions in octahedral sites, while P-type materials accommodate the alkali ions in prismatic sites. The most common structures for layered sodium-based transition metal oxides are O3, P2 and P3-type, whereby the number indicates the number of transition metal layers in the repeating cell unit.[16,17] Transition metal layered oxides have attractive properties as cathode materials for sodium-ion batteries, such as the ease of the synthesis and the high feasibility and reversibility of the sodium shuttling process, thus allowing a good overall electrochemical performance.[18]

Among the cathode candidates, single transition-metal layered oxides Na_xMO_2 (M = V, Cr, Mn, Fe, Co, Ni)[19−23] have been studied, although the initial investigations resulted in poor specific capacity and low retention. It has been demonstrated that nanostructured materials in combination with proper electrolyte solutions may be a valid approach to

Received: November 17, 2014
Accepted: February 18, 2015
Published: February 18, 2015

DOI: 10.1021/am5080437
ACS Appl. Mater. Interfaces 2015, 7, 5206−5212

overcome the above-mentioned issues.[24−27] Furthermore, it has been reported that the intermixing of transition metals in the MO_2-sheets improves the structural stability and electrochemical cycling performance. Indeed, these substituted layered sodium-based oxides represent suitable electrode materials for the use in sodium-ion batteries.[28−30] Manganese and iron-based materials are of particular interest due to the high elemental abundance and low cost, as well as the promising performance of the electrodes including them as doping elements. In addition, nickel is also known to be very beneficial for the electrochemical performance, due to the Ni^{2+}/ Ni^{4+} redox process,[30] but yet, no detailed study has been performed on how its content affects the electrochemical properties of Na_xMO_2 (M = Ni, Fe, Mn). Herein, we present a comparative study on the impact of the Ni/Fe ratio, annealing temperature and stoichiometric sodium content during synthesis on the structural, morphological and electrochemical properties of various layered compounds of the type Na_xMO_2 (M = Ni, Fe, Mn). The target of this study is to reveal how the parameters affect the material properties or, by implication, how different materials can be synthesized by varying these parameters, which is valuable for the development of the synthesis and the design of layered cathode materials for sodium-ion batteries (SIBs).

EXPERIMENTAL SECTION

Material Synthesis and Characterization. All the samples were synthesized by a solid-state reaction between sodium hydroxide (NaOH pellets Sigma-Aldrich >98%) and nickel−iron-manganese precursors. The precursors were prepared by coprecipitation method.[30] Accordingly, stoichiometric proportions of $NiSO_4{\cdot}6H_2O$ (Sigma-Aldrich, ACS reagent 99%), $FeSO_4{\cdot}7H_2O$ (AnalaR NORMAPUR, analytical reagent), and $MnSO_4{\cdot}5H_2O$ (AnalaR NORMAPUR, analytical reagent) were dissolved in water according to the desired Ni/Fe ratio content. An aqueous solution of NaOH (50% excess) was added dropwise to obtain the precursors. After extensive washing with distilled water, the precursors $[Ni_xFe_yMn_z](OH)_2$ were dried overnight at 120 °C. After grinding, the precursors were mixed with 0.685 equiv of sodium precursor (NaOH powder from ground NaOH pellets). The mixtures were pre-annealed in air atmosphere at 500 °C for 5 h (5 °C/min). All materials have been subjected to a final thermal treatment at 900 °C for 5 h (5 °C/min) followed by a water rinsing process. The layered compounds' general formula was $Na_xNi_yFe_zMn_{0.66}O_2$, and the materials had different Ni/Fe ratios. Following these conditions, five materials have been characterized: $Na_{0.6}Ni_{0.22}Fe_{0.11}Mn_{0.66}O_2$, $Na_{0.6}Ni_{0.155}Fe_{0.155}Mn_{0.66}O_2$, $Na_{0.5}Ni_{0.11}Fe_{0.22}Mn_{0.66}O_2$, $Na_{0.5}Ni_{0.05}Fe_{0.255}Mn_{0.66}O_2$, and $Na_{0.4}Fe_{0.33}Mn_{0.66}O_2$.

Additionally, $Na_{0.6}Ni_{0.22}Fe_{0.11}Mn_{0.66}O_2$, was prepared at annealing temperatures of 900, 850, and 800 °C to check the influence of the thermal treatment on the material structure. The synthesis of the $Na_{0.6}Ni_{0.22}Fe_{0.11}Mn_{0.66}O_2$ at 800 °C was repeated by changing the amount of initial sodium precursor from 0.685 to 1.0 equiv. Afterward, all the materials (NFMs compounds) were subjected to a water treatment (1 g of material was stirred in 100 mL of distilled water at 25 °C for 5 min).[29−31] Finally, all the obtained materials were dried at 120 °C for 24 h, ground and stored under inert atmosphere. We may assume, considering the synthesis conditions (high temperature in air atmosphere) and literature data that the oxidation state of the transition metals are (+II), (+III), and (+IV), respectively, for Ni, Fe, and Mn. The sodium content and the transition metal ratio in the samples were detected by inductively coupled plasma optical emission spectrometry with a Spectro ARCOS ICP-OES (Spectro Analytical Instruments, Kleve, Germany) instrument with axial plasma viewing.

The crystalline structure of the samples was detected by X-ray diffraction (XRD, Bruker D8 Advance, Germany) using the Cu Kα radiation in the 2θ range from 10° to 90°. Field emission scanning electron microscopy analysis (FE-SEM, Zeiss Auriga) was performed to get a morphological overview.

Electrochemical Characterization. We prepared electrodes by mixing the active material (85 wt %) with carbon black (Super C65, TIMCAL, 10 wt %) and polivinylidene fluoride PVDF, (6020 Solef, Arkema Group, 5 wt %). The slurries were made by adding an appropriate amount of *N*-methyl-2-pyrrolidone (NMP). After 2 h of intimate mixing, the resulting slurry was cast onto Al foil and dried at 120 °C. Punching and pressing of the electrodes (12 mm diameter) has followed. The mass loading of the electrodes was about 3 mg cm^{-2} (2.55 mg cm^{-2} active material). Sodium metal was used as counter and reference electrodes. The sodium was cut from sodium pieces (99.8%, Acros Organics), pressed, and finally punched on the current collector.

The electrodes were assembled into Swagelok-type sodium cells with 1 M $NaPF_6$ in PC as electrolyte solution, which was soaked into a glass fiber (Whatman) separator. Cells were assembled in an argon-filled glovebox with a H_2O and O_2 content lower than 1 ppm. Cyclic voltammetry tests were performed using a scan rate of 0.1 mV s^{-1} in the 4.6−1.5 V (vs Na/Na^+) potential range at 20 °C ± 2 °C using a VMP multichannel potentiostatic−galvanostatic system (Biological Science Instrument, France). The cells were cycled galvanostatically at 15 mA g^{-1} within 4.6−1.5 V voltage range at 20 °C ± 2 °C using Maccor series 4000 battery tester (U.S.A).

RESULTS AND DISCUSSION

Figure 1 gives an overview on the structural and morphological properties of the five NFM samples with different Ni/Fe ratio via XRD and FE-SEM. The X-ray diffraction patterns reveal that all materials are characterized by a layered, P2-type structure belonging to the hexagonal $P6_3/mmc$ space group (ICSD-93469). The patterns corresponding to $Na_{0.6}Ni_{0.22}Fe_{0.11}Mn_{0.66}O_2$, $Na_{0.6}Ni_{0.155}Fe_{0.155}Mn_{0.66}O_2$, and $Na_{0.5}Ni_{0.11}Fe_{0.22}Mn_{0.66}O_2$ in Figure 1a−c, respectively, reveal the absence of crystalline impurities. Further decrease of nickel content, with corresponding increase of the iron content, is accompanied by the appearance of a reflection at lower angles in the patterns of $Na_{0.5}Ni_{0.05}Fe_{0.255}Mn_{0.66}O_2$ and $Na_{0.4}Fe_{0.33}Mn_{0.66}O_2$, reported in Figure 1d,e, respectively. These peaks can be attributed to the presence of the hydrated phases caused by the water rinsing process, intend to dissolve sodium carbonate impurities formed during the annealing process but also leading to a partial chemical desodiation. In fact, it has been demonstrated that water can intercalate into the layered structure, which leads to an increase of the interlayer distance and causes a shift of the (00*l*) reflections to lower angles. Accordingly, the two diffraction peaks at 14 and 28°, which are marked by asterisks in Figure 1d,e, may be indexed as (002′) and (004′), respectively.[32,33] The presence of intercalated water can be explained considering the lower amount of sodium within compounds with higher content of Fe.

Indeed, a lower amount of sodium results in increased repulsion of neighboring oxygen layers. Water intercalation during the rinsing process takes place to reduce the overall energy. The water intercalation, however, is not energetically favored for larger sodium contents. Furthermore, it cannot be excluded that the absence of shifted reflections in the samples with increased Ni content (XRD in Figure 1a−c) may be attributed to the Ni-superlattice ordering action that hinders the water intercalation upon rinsing.[32,34] The FE-SEM images of the X-ray diffractograms (Figure 1, insets) clearly show the well-defined morphology typical of layered structure, characterized by a series of planes forming a single particles with an average dimension ranging from 1 to 2 μm. The figure shows the presence of trace impurities of sodium carbonates, minor

DOI: 10.1021/am5080437
ACS Appl. Mater. Interfaces 2015, 7, 5206−5212

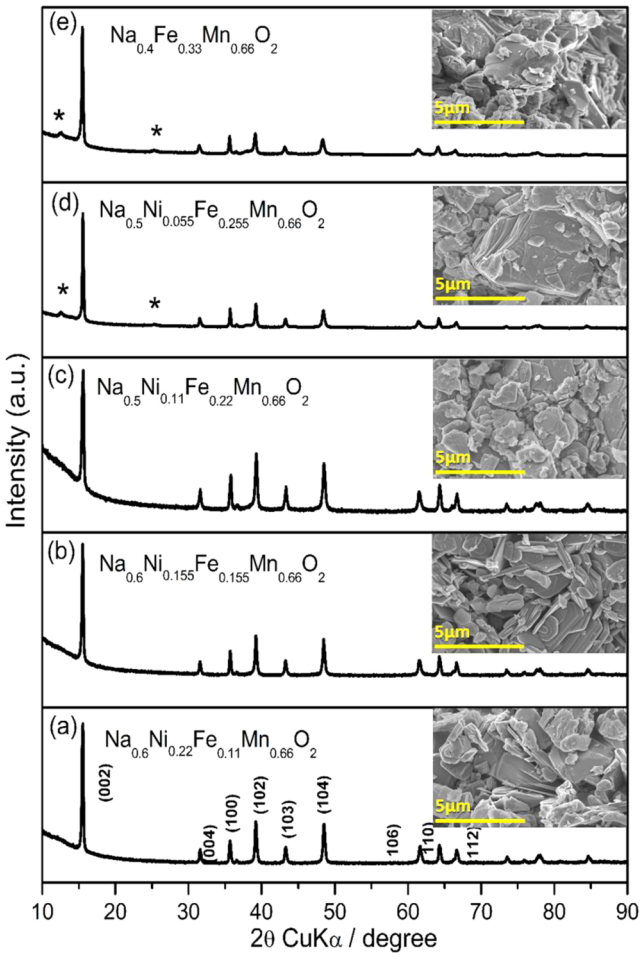

Figure 1. XRD patterns and (insets) FE-SEM images of P2-type NFM compounds with different Ni to Fe ratio. (a) $Na_{0.6}Ni_{0.22}Fe_{0.11}Mn_{0.66}O_2$, (b) $Na_{0.6}Ni_{0.155}Fe_{0.155}Mn_{0.66}O_2$, (c) $Na_{0.5}Ni_{0.11}Fe_{0.22}Mn_{0.66}O_2$, (d) $Na_{0.5}Ni_{0.05}Fe_{0.255}Mn_{0.66}O_2$, (e) $Na_{0.4}Fe_{0.33}Mn_{0.66}O_2$.

differences in particle size and negligible effects of the intercalated water in the samples with lower Ni content. Furthermore, the above-mentioned Ni-superlattice ordering effect (samples in Figure 1a−c) allows a well-defined layered structure, more pronounced in respect to the other samples.

Figure 2a reports the cyclic voltammetry (CV) tests of the various NaNFM samples in sodium half cells, performed to study the influence of the Ni/Fe ratio on the electrochemical behavior of the electrode. The voltammograms show the typical peaks associated with the electrochemical sodium (de)-intercalation process into the layered structure, involving reversible processes in the 2−4 V potential region and phase change at the higher potential values. All samples exhibit a reversible redox process at about 2.0 V vs Na/Na^+, i.e. higher sodium contents, due to the Mn^{4+}/Mn^{3+} redox process and corresponding structural rearrangement of the layers[35,36] and the two-phase oxidation reaction associated with the formation of the O2-phase, resulting from the gliding of the layers at very low sodium content (4.2 V vs Na/Na^+).[13] The sample with the higher nickel content ($Na_{0.6}Ni_{0.22}Fe_{0.11}Mn_{0.66}O_2$ in panel I) shows the reversible peaks between 3.2 and 3.9 V vs Na/Na^+, attributed to the Ni^{2+}/Ni^{4+} redox couple, with a double-electron process involving changes in the layer alignment in the material and structural reorganization due to sodium vacancy ordering, with consequent change in the peak shape and final stabilization upon cycling (see region marked by the green circle in Figure 2a, panel I). Figure 2a, panels II−IV show that the progressive increase of the Fe content and the corresponding decrease of the Ni content lead to the shift of the peaks associated with the above-mentioned Ni^{2+}/Ni^{4+} redox process to lower voltage (see region marked by the green dotted-line in panels I−IV). As expected, the Ni-free sample ($Na_{0.4}Fe_{0.33}Mn_{0.66}O_2$ in panel V) does not show peaks in the 3.2−3.9 V potential region but the appearance of reversible peaks at lower voltage (i.e., around 3 V) most likely due to the Fe^{2+}/Fe^{3+} redox couple (see regions marked by the red circle in Figure 2a, panel V, and by the corresponding red dotted line). Furthermore, the voltammograms reveal that an increasing Fe content leads to an increase of the intensity and a slight shift to lower voltages of the peak corresponding to the Mn^{4+}/Mn^{3+} redox process at 2 V. This is due to the charge compensation, which implies an increased amount of redox active manganese at lower Ni^{2+} contents. We can reasonably assume that Ni doping stabilizes the material due to a minor Mn^{3+} formation with consequent improvement of the energy efficiency of the (de)sodiation process. The suitability of the P2-NFMs as cathode materials is verified in terms of galvanostatic cycling in sodium metal half cells. Figure 2b reports the voltage profiles and cycling behavior of the different materials (insets). All materials deliver high capacities, typical for P2-type layered compounds. Ni-rich $Na_{0.6}Ni_{0.22}Fe_{0.11}Mn_{0.66}O_2$ material reveals a first discharge capacity of 205 mAh g^{-1} and 178 mAh g^{-1} after 30 cycles, corresponding to a capacity retention of about 86%. Similarly, Ni-free $Na_{0.4}Fe_{0.33}Mn_{0.66}O_2$ shows a first delivered capacity of about 200 and 174 mAh g^{-1} after 30 cycles with a capacity retention of about 87%. Hence, the most relevant difference between the various samples in Figure 2 seems to be the energy efficiency and potential at which the capacity is delivered (i.e. moving to higher values by increasing the Ni-content), thus suggesting that the Ni-rich sample $Na_{0.6}Ni_{0.22}Fe_{0.11}Mn_{0.66}O_2$ to provide higher energies. The cycling behavior of the different materials in the first 30 cycles is similar to our previous observations for the long-term cycling of $Na_{0.5}Ni_{0.23}Fe_{0.13}Mn_{0.63}O_2$ at higher C-rate, suggesting similar long-term cyclability.[30]

Figure 3 reports the effect of annealing temperature (either 800, 850, or 900 °C) on the structural and electrochemical characteristics of the sample with the most promising performance, i.e. $Na_{0.6}Ni_{0.22}Fe_{0.11}Mn_{0.66}O_2$. The XRD pattern in Figure 3a, reveals the material prepared at 900 °C to be of P2-type layered structure (space group: $P6_3/mmc$). The Rietveld refinement using the hexagonal unit cell leads to an intralayer distance (M−M) of a = 2.88 Å and an interlayer distance of c = 11.2 Å. The FE-SEM image reported as inset in Figure 3a clearly shows the platelet like micrometric morphology, characterized by a sequence of smooth facets. The XRD pattern of the sample prepared at 850 °C is reported in Figure 3b and reveals that the lower annealing temperature induces the formation of a new phase (i.e., P3). Indeed, the Rietveld refinement of the pattern indicates a mix of P2 and P3 phases, with about 40% content of the former phase. The material with P2−P3 structure reveals a different morphology, including the particle size. The FE-SEM image reveals a smaller submicrometric particles size for the mixed P2−P3 phase in comparison with the pure P2 phase. The NaNFM samples prepared at 800 °C (Figure 3c), show that a further decrease of the annealing temperature of 50 °C leads to the formation of a pure P3-type structure with $R\bar{3}m$ space group. The latter may

DOI: 10.1021/am5080437
ACS Appl. Mater. Interfaces 2015, 7, 5206−5212

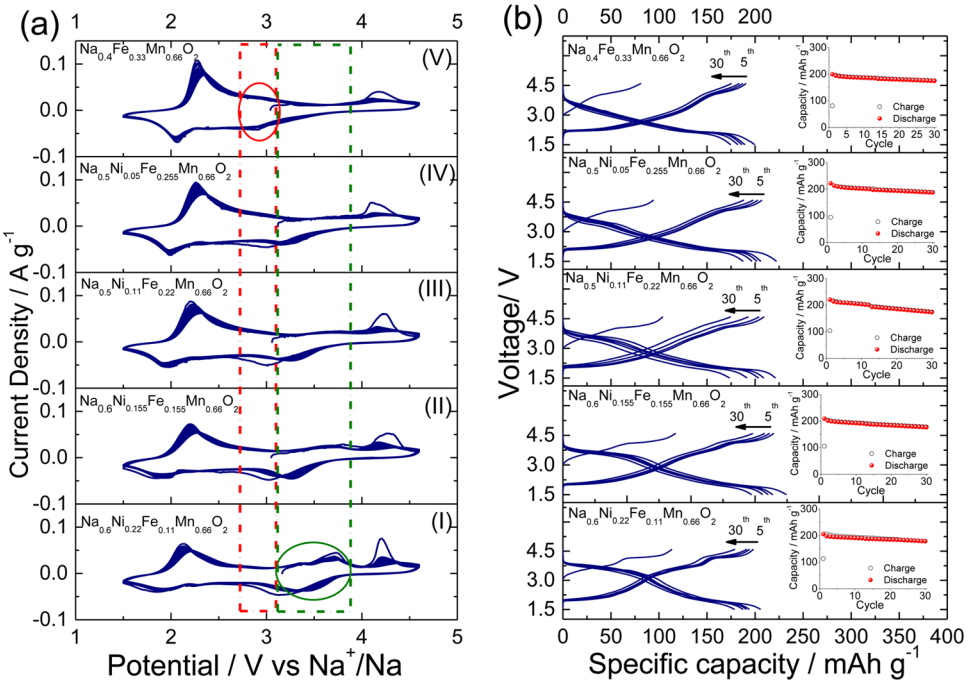

Figure 2. (a) Cyclic voltammetry test performed using P2-type layered materials obtained at 900 °C in sodium cells. (I) $Na_{0.6}Ni_{0.22}Fe_{0.11}Mn_{0.66}O_2$, (II) $Na_{0.6}Ni_{0.155}Fe_{0.155}Mn_{0.66}O_2$, (III) $Na_{0.5}Ni_{0.11}Fe_{0.22}Mn_{0.66}O_2$, (IV) $Na_{0.5}Ni_{0.05}Fe_{0.255}Mn_{0.66}O_2$, and (V) $Na_{0.4}Fe_{0.33}Mn_{0.66}O_2$. Tests performed using a scan rate of 0.1 mV sec^{-1} within the 1.5−4.6 V potential range. Counter and reference electrode of Na. Temperature: 20 °C ± 2 °C. Electrolyte: 1 M $NaPF_6$ in PC. (b) Cycling performances of the above-mentioned electrodes in sodium cells in terms of voltage profiles and cycling behavior (inset). Tests run at 15 mA g^{-1} within the 1.5−4.6 V voltage range. Counter and reference electrode of Na. Temperature: 20 °C ± 2 °C. Electrolyte: 1 M $NaPF_6$ in PC.

be refined using the rhombohedral unit cell leading to an intralayer distance (M−M) of a = 2.88 Å and an interlayer distance of c = 16.9 Å, while the FE-SEM inset of Figure 3c reveals nanometric particle size.

The potential profiles of the first cycle as well as the capacities and corresponding Coulombic efficiencies obtained during galvanostatic cycling are shown in Figure 3d for the different $Na_{0.6}Ni_{0.22}Fe_{0.11}Mn_{0.66}O_2$ samples. The $Na_{0.6}Ni_{0.22}Fe_{0.11}Mn_{0.66}O_2$ samples prepared at 800 °C, 850 °C and 900 °C reveal only a minor difference in terms of the first charge capacity (121, 110, and 113 mAh g^{-1}, respectively). However, in the subsequent discharge process the delivered capacity differs significantly (234, 216, and 205 mAh g^{-1}, respectively). These results might suggest that the P3-type structured material, synthesized at the lower temperature, exhibit the best overall electrochemical performance. However, the cycling behavior (Figure 3d, inset) is clear evidence to the contrary. After 30 cycles, a discharge capacity of 176, 129, and 178 mAh g^{-1} is delivered for the pure P3-type (800 °C), mixed P2−P3-type (850 °C) and P2-type (900 °C) material, corresponding to a capacity retention of 75, 60, and 87%, respectively. These results clearly indicate that the higher initial capacity is also interconnected with a higher capacity fade. Consequently, the most stable cycling behavior is achieved by the P2-type structured layered oxide. The different electrochemical performances of the samples most probably do not originate from the different structure but are rather induced by the morphological features and, in particular, the particle size. The P3 phase, characterized by remarkably smaller particles, shows a high initial capacity but pronounced fading upon cycling and lower efficiency (99.2%), while the P2 phase characterized by bigger particles evidences lower initial capacity, greater stability and higher efficiency (99.7%). In fact, it has been reported that the low stability of the P3 phase may be attributed to a more pronounced manganese dissolution, a phenomenon often present in Mn based layered materials and further accelerated by the presence of very small or nanosized particles.[37] Nevertheless, although this explains the different performance of the pure P2-type and P3-type phase, the mixed structure is clearly not revealing an intermediate but a much lower cycling stability, indicating a continuous active material degradation process to be present. In fact, this observation is in line with the results reported for mixed P2/P3-type $Na_xNi_{0.22}Co_{0.11}Mn_{0.66}O_2$, in which a strong manganese dissolution was present in organic carbonate based electrolytes.[37] This somewhat indicates mixed P2/P3-type structured materials are not suitable active materials in this electrolytic solution.

The samples reported in Figures 1−3 were prepared by using a stoichiometric sodium content of 0.685 equiv during the synthesis. The stoichiometries of the final compounds, as detected by ICP, indicate a sodium content varying from 0.6 to 0.4 equiv, suggesting partial loss of Na during the temperature annealing and water rinsing processes. Figure 3 demonstrated the annealing at 900 °C to lead to the P2-type phase while annealing at 800 °C results into the P3 structure. However, in the following, we demonstrate that a P2-type structure phase can be also obtained at lower temperatures via increasing the stoichiometric sodium content. Figure 4 reports the measured and calculated XRD patterns of the layered $Na_xNi_{0.22}Fe_{0.11}Mn_{0.66}O_2$ materials annealed at 800 °C and using either (a) 0.685 or (b) 1.0 equiv of sodium. The sample prepared with lower sodium content crystallizes into a P3 structure (space group $R\bar{3}m$), while the material using an excess

DOI: 10.1021/am5080437
ACS Appl. Mater. Interfaces 2015, 7, 5206−5212

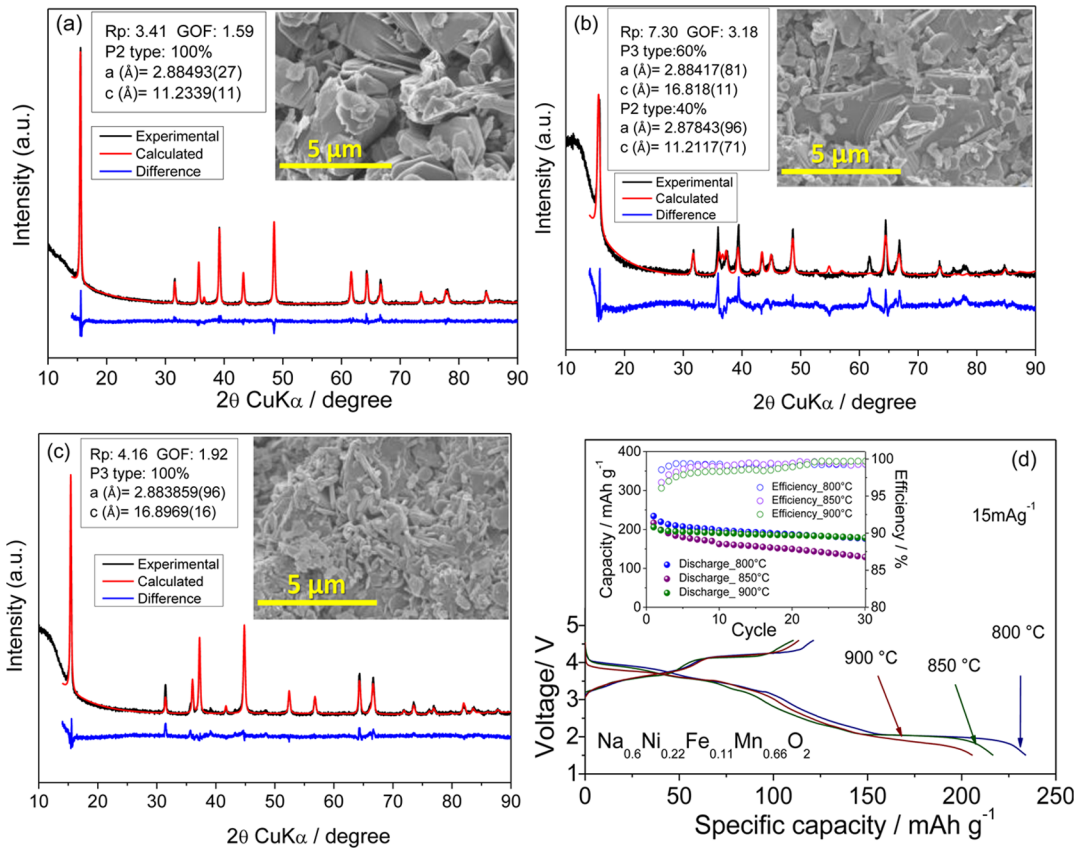

Figure 3. (Black line) Experimental and (red line) calculated XRD diffraction patterns of a $Na_{0.6}Ni_{0.22}Fe_{0.11}Mn_{0.66}O_2$ material prepared using the annealing temperature of (a) 900 °C (pure P2), (b) 850 °C (mixed P2−P3), and (c) 800 °C (pure P3); (insets) respective FE-SEM images. (d) Comparison of the first charge−discharge voltage profile and (inset) cycling behavior and efficiency of sodium cells using the NFM compounds prepared at 900, 850, and 800 °C. Tests run at 15 mA g^{-1} within the 1.5−4.6 V voltage range. Counter and reference electrode of Na. Temperature: 20 °C ± 2 °C. Electrolyte: 1 M $NaPF_6$ in PC.

of sodium reveals the typical P2 structure with space group $P6_3/mmc$. Figure 4c,d illustrates the potential profiles, capacities, and efficiencies obtained during galvanostatic cycling of the P3-NaNFM and P2-NaNFM electrodes, respectively. The P3−$Na_xNi_{0.22}Fe_{0.11}Mn_{0.66}O_2$ electrode delivers 121 mAh g^{-1} during the first charge and 234 mAh g^{-1} in the following discharge, while the P2−$Na_xNi_{0.22}Fe_{0.11}Mn_{0.66}O_2$ exhibits lower capacities of 113 and 208 mAh g^{-1} during the first charge and discharge, respectively. Both materials show a good overall cycling behavior, but the better performance is evidenced by the P2-type layered electrode, as already demonstrated by Figure 3, reporting the samples synthesized at various temperatures. In more detail, the P2-type material exhibits a slightly better energy efficiency of the (de)sodiation process, higher Coulombic efficiencies (99.3 vs 99.1% for the P3-type analogue) and a much better capacity retention upon cycling (82.1 vs 75.5% after 30 cycles). Thus, a higher sodium content in the synthesis allows a reduction of the annealing temperature, while the P2-type material with the better intrinsic electrochemical properties can still be obtained. This represents a remarkable result that might enable a further cost reduction for the synthesis of layered materials, as cost represents such an important issue for SIBs. The cathode materials here reported show an issue associated with sodium deficiency that may lead to sodium-ion full cell balance. This drawback may be mitigated by chemical or electrochemical activation process before the use of the electrodes in a full cell. Possible preactivation of the anode material leading to an extra amount of sodium may be performed by chemical sodiation procedure involving direct contact of the anode with sodium metal wet by the electrolyte prior its use in full cell.[38]

CONCLUSION

In this work, we reported a deep study on layered transition metal oxides Na_xMO_2 (M = Ni, Fe, Mn) for their use as cathode materials in sodium-ion batteries. The materials have been prepared through an optimized synthetic route involving coprecipitation method, annealing process in air and a water-rinsing process. The effect of the Ni-to-Fe ratio, the annealing temperature and stoichiometric sodium content during the synthesis have been investigated as parameters affecting the electrochemical properties of the prepared oxides. We demonstrated via a comparative study that these factors play a crucial role for the materials structure and morphology, thus leading to a different electrochemical behavior. The data indicated that higher annealing temperatures (900 °C, 0.685 equiv of Na^+), as well as stoichiometric sodium content employed during the synthesis (800 °C, 1.0 equiv of Na^+), promote P2-phase formation, while lower temperatures and lower sodium amount enable the formation of P3-type phase (800 °C, 0.685 equiv of Na^+). The reported results indicated that different Ni to Fe ratio only slightly affects the good electrochemical behavior of the P2-type layered electrodes in terms of delivered capacity, while the nickel content remarkably influences the working potential. Moreover, we demonstrated

DOI: 10.1021/am5080437
ACS Appl. Mater. Interfaces 2015, 7, 5206−5212

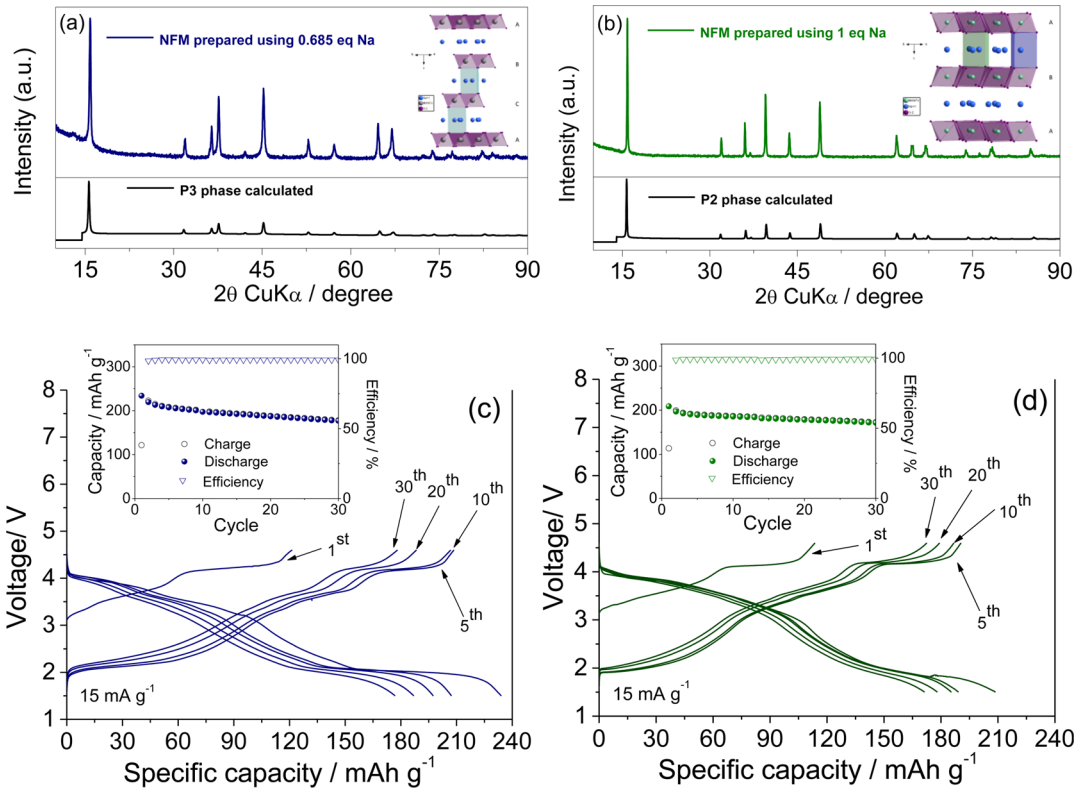

Figure 4. XRD patterns of $Na_xNi_{0.22}Fe_{0.11}Mn_{0.66}O_2$ obtained at 800 °C with different amounts of Na equivalent: (a) 0.685 and (b) 1. Voltage profiles and (insets) cycle life of sodium cells using a $Na_xNi_{0.22}Fe_{0.11}Mn_{0.66}O_2$ electrode obtained at 800 °C using (c) 0.685 equiv of Na and (d) 1 equiv of Na. Tests run at 15 mA g^{-1} within the 1.5−4.6 V voltage range. Counter and reference electrode of Na. Temperature: 20 °C ± 2 °C. Electrolyte: 1 M $NaPF_6$ in PC.

that increased Ni content in the transition metal layers can improve the energy efficiency of the (de)sodiation process and, finally, hinder the Mn dissolution. It has been demonstrated that P-type layered oxides, in particular Ni-rich ones, are suitable cathode materials for sodium-ion batteries in view of the high delivered capacities of about 200 mAh g^{-1}. Furthermore, the data evidenced that the well-defined structure and the favorable morphological properties of the P2-layered electrode allow better electrochemical performances in terms of cycling stability compared with the P3-type electrode.

AUTHOR INFORMATION

Corresponding Authors

*E-mail: jusef.hassoun@uniroma1.it.
*E-mail: stefano.passerini@kit.edu.

Notes

The authors declare no competing financial interest.

ACKNOWLEDGMENTS

I.H. and J.H. would like to thank the support of the Italian project "Regione Lazio" at Sapienza University of Rome, Chemistry Department. D.B. and S.P. acknowledges the financial contribution of BMW AG.

REFERENCES

(1) Scrosati, B.; Hassoun, J.; Sun, Y.-K. Lithium-Ion Batteries. A Look into the Future. *Energy Environ. Sci.* **2011**, *4*, 3287−3295.

(2) Tarascon, J.-M.; Armand, M. Issues and Challenges Facing Rechargeable Lithium Batteries. *Nature* **2001**, *414*, 359−367.

(3) Tarascon, J.-M. Is Lithium the New Gold? *Nat. Chem.* **2010**, *2*, 510−510.

(4) Jaskula, B. W. Lithium, In *Mineral Commodity Summaries* 2012, U.S. Geological Survey, Reston, VA,2012, 94.

(5) Palomares, V.; Serras, P.; Villaluenga, I.; Hueso, K. B.; Carretero-Gonzalez, J.; Rojo, T. Na-Ion Batteries, Recent Advances and Present Challenges to Become Low Cost Energy Storage Systems. *Energy Environ. Sci.* **2012**, *5*, 5884−5901.

(6) Kim, S.-W.; Seo, D.-H.; Ma, X.; Ceder, G.; Kang, K. Electrode Materials for rechargeable Sodium-Ion Batteries: Potential Alternatives to Current Lithium-Ion Batteries. *Adv. Energy Mater.* **2012**, *2*, 710−721.

(7) Abraham, K. M. Intercalation Positive Electrodes for Rechargeable Sodium Cells. *Solid State Ionics* **1982**, *7*, 199−212.

(8) West, K.; Zachau-Christiansen, B.; Jacobsen, T.; Skaarup, S. J. Solid-state Sodium Cells—An Alternative to Lithium Cells? *J. Power Sources* **1989**, *26*, 341−345.

(9) Delmas, C.; Braconnier, J. J.; Fouassier, C.; Hagenmuller, P. Electrochemical Intercalation of Sodium in Na_xCoO_2 Bronzes. *Solid State Ionics* **1981**, *3*−*4*, 165−169.

(10) Nagelberg, A. S.; Worrell, W. L. A Thermodynamic Study of Sodium-Intercalated TaS_2 and TiS_2. *J. Solid State Chem.* **1979**, *29*, 345−354.

(11) Komaba, S.; Yabuuchi, N.; Nakayama, T.; Ogata, A.; Ishikawa, T.; Nakai, I. Study of the Reversible Electrode Reaction of $Na_{1-x}Ni_{0.5}Mn_{0.5}O_2$ for Rechargeable Sodium-ion Battery. *Inorg. Chem.* **2012**, *51*, 6211−6220.

(12) Sathiya, M.; Hemalatha, K.; Ramesha, K.; Tarascon, J.-M.; Prakash, A. S. Synthesis, Structure, and Electrochemical Properties of the Layered Sodium Insertion Cathode Material: $NaNi_{1/3}Mn_{1/3}Co_{1/3}O_2$. *Chem. Mater.* **2012**, *24*, 1846−1853.

(13) Lu, Z.; Dahn, J. R. In Situ X-Ray Diffraction Study of P2-$Na_{2/3}Ni_{1/3}Mn_{2/3}O_2$. *J. Electrochem. Soc.* **2001**, *148*, A1225−A1229.

(14) Wu, L.; Bresser, D.; Buchholz, D.; Giffin, G.; Ramirez Castro, C.; Ochel, A.; Passerini, S. Unfolding the Mechanism of Sodium

DOI: 10.1021/am5080437
ACS Appl. Mater. Interfaces 2015, 7, 5206−5212

Insertion in Anatase TiO_2 Nanoparticles. *Adv. Energy Mater.* **2014**, DOI: 10.1002/aenm.201401142.
(15) Ponrouch, A.; Goñi, A. R.; Palacín, M. Rosa High Capacity Hard Carbon Anodes for Sodium ion Batteries in Additive Free Electrolyte. *Electrochem. Commun.* **2013**, *27*, 85−88.
(16) Fouassier, C.; Delmas, C.; Hagenmuller, P. Evolution Structurale et Proprietes Physiques des Phases A_xMO_2 (A = Na, K; M = Cr, Mn, Co) ($x \leq 1$). *MRS Bull.* **1975**, *10*, 443−449.
(17) Delmas, C.; Fouassier, C.; Hagenmuller, P. Structural Classification and Properties of Layered Oxides. *Physica* **1980**, *99*, 8.
(18) Kubota, K.; Yabuuchi, N.; Yoshida, H.; Dahbi, M.; Komaba, S. Layered Oxides as Positive Electrode Materials for Na-ion Batteries. *MRS Bull.* **2014**, *39*, 416−422.
(19) Hamani, D.; Ati, M.; Tarascon, J.-M.; Rozier, P. Na_xVO_2 as Possible Electrode for Na-Ion Batteries. *Electrochem. Commun.* **2011**, *13*, 938−941.
(20) Komaba, S.; Takei, C.; Nakayama, T.; Ogata, A.; Yabuuchi, N. Electrochemical Intercalation Activity of Layered $NaCrO_2$ vs $LiCrO_2$. *Electrochem. Commun.* **2010**, *12*, 355−358.
(21) Caballero, A.; Hernán, L.; Morales, J.; Sánchez, L.; Santos Peña, J.; Aranda, M. A. G. Synthesis and Characterization of High-temperature Hexagonal P2-$Na_{0.6}MnO_2$ and its Electrochemical Behaviour as Cathode in Sodium Cells. *J. Mater. Chem.* **2002**, *12*, 1142−1147.
(22) Yabuuchi, N.; Yoshida, H.; Komaba, S. Crystal Structures and Electrode Performance of Alpha-$NaFeO_2$ for Rechargeable Sodium Batteries. *Electrochemistry* **2012**, *80*, 716−719.
(23) Vassilaras, P.; Ma, X.; Li, X.; Ceder, G. Electrochemical Properties of Monoclinic $NaNiO_2$. *J. Electrochem. Soc.* **2013**, *160*, A207−A211.
(24) Su, D.; Wang, C.; Ahn, H.-J.; Wang, G. Single Crystalline $Na_{0.7}MnO_2$ Nanoplates as Cathode Materials for Sodium-Ion Batteries with Enhanced Performance. *Chem.—Eur. J.* **2013**, *19*, 10884−10889.
(25) Su, D.; Wang, G. Single-Crystalline Bilayered V2O5 Nanobelts for High-Capacity Sodium-Ion Batteries. *ACS Nano* **2013**, *7*, 11218−11226.
(26) Su, D.; Ahn, H.-J.; Wang, G. β-MnO_2 Nanorods with Exposed Tunnel Structures as High-Performance Cathode Materials for Sodium-Ion Batteries. *NPG Asia Mater.* **2013**, *5*, e70.
(27) Ding, J. J.; Zhou, Y. N.; Sun, Q.; Yu, X. Q.; Yang, X. Q.; Fu, Z. W. Electrochemical Properties of P2-Phase $Na_{0.74}CoO_2$ Compounds as Cathode Material for Rechargeable Sodium-Ion Batteries. *Electrochim. Acta* **2013**, *87*, 388−393.
(28) Yabuuchi, N.; Kajiyama, M.; Iwatate, J.; Nishikawa, H.; Hitomi, S.; Okuyama, R.; Usui, R.; Yamada, Y.; Komaba, S. P2-Type $Na_x[Fe_{1/2}Mn_{1/2}]O_2$ Made from Earth-Abundant Elements for Rechargeable Na Batteries. *Nat. Mater.* **2012**, *11*, 512−517.
(29) Buchholz, D.; Moretti, A.; Kloepsch, D.; Nowak, S.; Siozios, V.; Winter, M.; Passerini, S. Toward Na-Ion Batteries-Synthesis and Characterization of a Novel High Capacity Na Ion Intercalation Material. *Chem. Mater.* **2013**, *25*, 142−148.
(30) Hasa, I.; Buchholz, D.; Passerini, S.; Scrosati, B. High Performance $Na_{0.5}[Ni_{0.23}Fe_{0.13}Mn_{0.63}]O_2$ Cathode for Sodium-Ion Batteries. *J. Adv. Energy Mater.* **2014**, DOI: 10.1002/aenm.201400083.
(31) Buchholz, D.; Chagas, L. G.; Winter, M.; Passerini, S. P2-Type Layered $Na_{0.45}Ni_{0.22}Co_{0.11}Mn_{0.66}O_2$ as Intercalation Host Material for Lithium and Sodium Batteries. *Electrochim. Acta* **2013**, *110*, 208−213.
(32) Lu, Z.; Dahn, J. R. Intercalation of Water in P2, T2, and O2 Structure $A_z[Co_xNi_{1/3-x}Mn_{2/3}]O_2$. *Chem. Mater.* **2001**, *13*, 1252−1257.
(33) Buchholz, D.; Gomes Chagas, L.; Vaalma, C.; Wu, L.; Passerini, S. Water Sensitivity of Layered P2/P3−$Na_xNi_{0.22}Co_{0.11}Mn_{0.66}O_2$ Cathode Material. *J. Mater. Chem. A* **2014**, *2*, 13415−13421.
(34) Lu, Z.; Donaberger, R. A.; Dahn, J. R. Superlattice Ordering of Mn, Ni, and Co in Layered Alkali Transition Metal Oxides with P2, P3, and O3 Structures. *Chem. Mater.* **2000**, *12*, 3583−3590.
(35) Yuan, D.; Hu, X.; Qian, J.; Pei, F.; Wu, F.; Mao, R.; Ai, X.; Yang, H.; Cao, Y. P2-type $Na_{0.67}Mn_{0.65}Fe_{0.2}Ni_{0.15}O_2$Cathode Material with High-Capacity for Sodium-Ion Battery. *Electrochim. Acta* **2014**, *116*, 300−305.
(36) Thorne, J. S.; Dunlap, R. A.; Obrovac, M. N. Structure and Electrochemistry of $Na_xFe_xMn_{1-x}O_2$ ($1.0 \leq x \leq 0.5$) for Na-Ion Battery Positive Electrodes. *J. Electrochem. Soc.* **2013**, *160*, A361−A367.
(37) Gomes Chagas, L.; Buchholz, D.; Wu, L.; Vortmann, B.; Passerini, S. Unexpected Performance of Layered Sodium-Ion Cathode Material in Ionic Liquid-based Electrolyte. *J. Power Sources* **2014**, *247*, 377−383.
(38) Lee, D.-J.; Park, J.-W.; Hasa, I.; Sun, Y.-K.; Scrosati, B.; Hassoun, J. Alternative Materials for Sodium Ion−Sulphur Batteries. *J. Mater. Chem. A* **2013**, *1*, 5256−5261.

DOI: 10.1021/am5080437
ACS Appl. Mater. Interfaces 2015, 7, 5206−5212